THE JOURNAL OF PHYSICAL CHEMISTRY A
A JOURNAL OF THE AMERICAN CHEMICAL SOCIETY

pubs.acs.org/JPCA Article

Ro-vibrational Distribution of NO^+ Dissociated from NO_2^+ Ions in the a^3B_2 and b^3A_2 States: A Slow "Impulsive" Dissociation Example Revealed from Threshold Photoelectron–Photoion Coincidence Imaging

Published as part of The Journal of Physical Chemistry virtual special issue "Cheuk-Yiu Ng Festschrift".

Tongpo Yu, Xiangkun Wu, Xiaohan Ning, Yan Chen, Xiaoguo Zhou,* Xinhua Dai, Fuyi Liu, and Shilin Liu*

Cite This: *J. Phys. Chem. A* 2021, 125, 3316–3326 Read Online

ACCESS | Metrics & More | Article Recommendations

ABSTRACT: To clarify the contentions about dissociative photoionization mechanism of nitrogen dioxide via the a^3B_2 and b^3A_2 ionic states, a new threshold photoelectron–photoion coincidence (TPEPICO) velocity imaging has been conducted in the 12.8–14.0 eV energy range at the Hefei Light Source. The fine vibrational-resolved threshold photoelectron spectrum agrees well with the previous measurements. The ro-vibrational distributions of NO^+, as the unique fragment ion in the dissociation of NO_2^+ in specific vibronic levels of a^3B_2 and b^3A_2 states, are derived from the recorded TPEPICO velocity images. A "cold" vibrational ($v^+ = 0$) and "hot" rotational population is observed at the $a^3B_2(0,3,0)$ and (0,4,0) vibronic levels, while the dissociation of NO_2^+ in $b^3A_2(0,0,0)$ leads to the NO^+ fragment with both hot vibrational and rotational populations. With the aid of the quantum chemical calculations at the time-dependent B3LYP level, minimum energy paths on the potential energy surfaces of the a^3B_2 and b^3A_2 states clarify their adiabatic dissociation mechanisms near the thresholds, and this study proposes reliable explanations for the observed internal energy distributions of fragment ions. Additionally, this study provides valuable insights into the application of the classical "impulsive" model on an overall slow dissociation process.

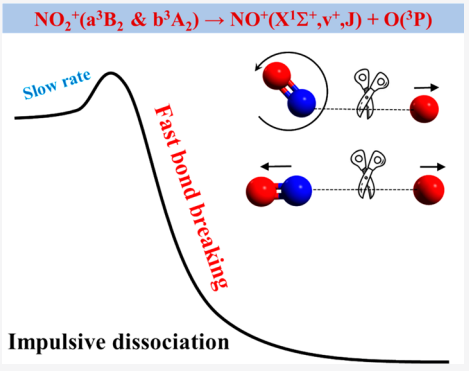

1. INTRODUCTION

As one of the key reactive species, nitrogen dioxide (NO_2) plays an important role in atmospheric chemistry.[1,2] Its cation, NO_2^+, is also an important intermediate in stratospheric ion–molecule reactions,[3] since the $O^+(^4S) + N_2$,[4] $N(^4S) + O_2^+$, and $N^+ + O_2$[5−10] reactions are the most significant sources of NO^+ and O^+ ions in planetary atmosphere.[11] Therefore, the properties of NO_2 neutral molecule and cation have attracted extensive attentions in past decades. However, there are still some inconsistent conclusions about the state of art dissociation dynamics of NO_2^+ in electronically excited states.

As an open-shell molecule, the neutral NO_2 has a C_{2v} symmetric bent geometry, with an valence electronic configuration of $[core](1b_1)^2(4b_2)^2(1a_2)^2(6a_1)^1$ in the ground electronic state, X^2A_1. When one electron is removed from the outer orbitals, $6a_1$, $4b_2$, and $1a_2$, two separate spin ionic states, a singlet and a triplet state, are naturally produced, except for $(6a_1)^{-1}$, thus leading to the NO_2^+ molecular ion in the $X^1\Sigma+g(^1A_1)$, a^3B_2, b^3A_2, A^1A_2, and B^1B_2 electronic states, respectively. To study NO_2^+ geometry in specific electronic states, He-I and He-II photoelectron spectroscopy,[12−15] threshold photoelectron (TPE) spectroscopy,[16,17] and pulsed-field-ionization zero kinetic energy (PFI-ZEKE) spectroscopy[18] were performed previously, together with a few theoretical calculations.[5,19,20] According to Franck–Condon factors and statistical factors, the band intensity of a triplet state was usually stronger than that of the corresponding singlet in photoelectron spectra.[21] For these low-lying electronic states, the spectral assignments were noncontroversial owing to their well separated spectral bands. For instance, the a^3B_2 state covers the energy range of 12.3–13.4 eV with a fine vibrational progression, while the b^3A_2 state is

Received: January 27, 2021
Revised: April 3, 2021
Published: April 16, 2021

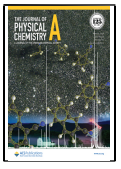

https://doi.org/10.1021/acs.jpca.1c00701
J. Phys. Chem. A 2021, 125, 3316–3326

located in the range of 13.4−13.9 eV, with the strongest 0−0 band and a few broadened vibrational peaks.[12]

Based on the assignments, the dissociation of NO_2^+ in these low-lying electronic states has been investigated with various experimental approaches, including electron ionization.[16,18,22] photofragment excitation spectroscopy,[23,24] photoionization mass spectrometry,[25,26] fast-ion beam laser spectroscopy,[27] photoelectron−photoion coincidence (PEPICO) spectroscopy,[13,17] and threshold photoelectron−photoion coincidence (TPEPICO) spectroscopy.[16] The $X^1\Sigma_g^+$state with a linear geometry has a deep potential well. The symmetric stretching (ν_1^+) and the bending (ν_2^+) vibrational frequencies were measured to be approximately 175 and 75 meV respectively.[13] NO_2^+ cation in the electronically excited states is unstable, and the NO^+, O^+, O_2^+, and N^+ fragment ions can be produced at different photon energies.[28] In fact, only two lowest dissociation channels of $NO^+(X^1\Sigma^+)$ + $O(^3P)$ and $NO^+(X^1\Sigma^+)$ + $O(^1D)$ correlate with those electronic states below 16 eV. The corresponding dissociation limits were determined at 12.3797 and 14.3471 eV, respectively, with taking into account the dissociation energy of NO_2 (D_0 = 3.1154 eV)[29] and the ionization energy of NO (IE = 9.2643 eV).[30] The lowest excited state, a^3B_2, was conformably found to be metastable in previous studies except for the vibrational ground state (0,0,0), since the parent ion and the NO^+ fragment ion were both observed at the vibrationally excited levels.[13] Yet, the reported lifetimes were quite different, *e.g.*, 5−155 μs in (ZEKE-PFI),[31] on a microsecond time scale suggested by Eland and Karlsson's PEPICO experiments,[13] and submilliseconds in Shibuya et al.'s TPEPICO measurement,[16] i.e. 1.35 ms for (0,0,0), 760 μs for (0,1,0), 66 μs for (0,2,0), and 42 μs for (0,3,0) levels. Different from the metastable a^3B_2 state, the second excited state, b^3A_2, was suggested to be repulsive due to the much wider vibrational peaks, and the NO^+ fragment ion was observed with large kinetic energies close to the energetic limit.[13] Moreover, the recoil angle for NO^+ fragments was verified to be ∼50° relative to the initial C_{2v} symmetry axis in dissociative photoionization of NO_2 via the b^3A_2 ionic state at 14.4 eV.[32] In recent imaging PEPICO studies,[17,33] the state-specific dissociative photoionization of NO_2^+ below 20 eV was systematically studied for the a^3B_2, b^3A_2, A^1A_2, B^1B_2, c^3B_1, C^1B_1, d^3A_1, e^3B_2, and D^1B_2 electronic states, respectively. The NO^+ fragment ions were observed at the ground vibrational level with a high rotational population, regardless of dissociation from $NO_2^+(a^3B_2,b^3A_2)$ cations.[17]

Although some experimental and theoretical investigations have been performed previously for the dissociation of NO_2^+ cations in the a^3B_2 and b^3A_2 states, there is still some controversy on their dissociation mechanisms. Hirst calculated the bending potential energy surface of a^3B_2 state and found a considerably deep well along the ON−O rupture.[5] A barrier of ∼0.8 eV was estimated to adiabatically correlate with the dissociation limit of $NO^+(X^1\Sigma^+)$ + $O(^3P)$, when fixing the bond angle at 120° and the unbroken N−O bond length at 1.22 Å. Due to its too higher than the experimental onset near the $a^3B_2(0,2,0)$ level in energy, a tunneling or an avoided crossing between two $^3B_2$ states was suggested for its dissociation mechanism by Eland et al.[12,13] However, such tunneling should be very weak for these NO^+ fragments and O atoms of heavy mass. The high-level CASPT2 calculations of Chang and Huang were opposed to the deduction of avoided crossing,[19] by checking the CASSCF wave functions "before" and "after" the barrier along the a^3B_2 N−O rupture. Instead, an intersystem crossing mechanism was proposed for the a^3B_2 dissociation by Shibuya et al.[16] Alternatively, Tang et al.[17] suggested that the coupling between the a^3B_2 state and the upper 2^3B_1 ionic state might be responsible for the dissociation of a^3B_2, since a curve crossing was calculated to be located at a bond angle of ∼90° along the bending potential curves of a^3B_2 and 2^3B_1 ionic states.[5]

To address this dispute, a new TPEPICO velocity imaging experiment has been performed for dissociative photoionization of NO_2 via the a^3B_2 and b^3A_2 ionic states in the photon energy range of 12.80−14.0 eV. In our TPEPICO velocity imaging experiment at the Hefei Light Source, the translation energy resolution ($\Delta E_T/E_T$ ∼ 3%)[34] can be achieved for ion imaging, so that the accurate kinetic energy released distribution (KERD) and angular distribution of NO^+ fragment ion can be obtained for a specific vibrational level in the both ionic states. Then, the ro-vibrational distribution can be assigned taking into account the dissociation limit and the spectroscopic parameters of NO^+. Moreover, the adiabatic potential energy surfaces of a^3B_2 and b^3A_2 along the ON−O bond length and θ(O−N−O) bond angle coordinates have been mapped using the time-dependent density functional theory (DFT). Consequently, the dissociation mechanisms of NO_2^+ in these both states are reliably uncovered. Although the classical "impulsive" model has always been used to describe a rapid dissociation along a repulsive potential energy surface, we shed light on its application on the overall relatively slow dissociation processes of NO_2^+ in a^3B_2 and b^3A_2.

2. EXPERIMENTAL AND COMPUTATIONAL SECTION

The experiment was performed on the BL09-U beamline of the Hefei Light Source. Details of the TPEPICO velocity imaging spectrometer and the beamline have been described previously;[34,35] thus, only a brief introduction is given here. VUV photons from an undulator of 800 MeV electron-storage ring were dispersed with a 6 m-long monochromator with a 370 grooves·mm^{-1} spherical grating, and the photon energy was covered from 7.5 to 22.5 eV with an energy-resolving power ($E/\Delta E$) of ∼2000 at 15 eV.[35] The absolute photon energies were calibrated using the well-known ionization energies of argon and xenon, leading to an uncertainty of 10 meV. A gas filter filled with argon was installed in front of the photoionization chamber to suppress higher-order harmonic radiation from the undulator. The photon flux was measured using a silicon photodiode (International Radiation Detectors, SXUV-100) to normalize TPE intensities.

The commercial NO_2 gas (99.9%) was used without any further purification. A continuous molecular beam (MB) of the mixed NO_2 and helium gas (1/10 v/v) with a stagnation pressure of 1.2 × 10^5 Pa was introduced into the chamber through a 20-μm-diameter nozzle, collimated by a 0.5-mm-diameter skimmer, and then intersected with the VUV beam at 10 cm downstream from the nozzle. The backing pressure was typically 5 × 10^{-5} Pa with the MB on. In the photoionization region, a dc electric field of ∼15 V·cm^{-1} extracted photoelectrons and photoions in opposite directions. A special ion optics was utilized to collect the photoelectrons and photoions simultaneously and map their velocity images,[34] where the electron image was significantly magnified owing to the delayed flight time. Then, a mask with a 1-mm-diameter hole and a concentric ring was placed in front of the electron detector to further subtract energetic electron contamination

https://doi.org/10.1021/acs.jpca.1c00701
J. Phys. Chem. A 2021, 125, 3316−3326

in TPES as described previously.[36] The TPEPICO measurements were performed with a single-start multiple-stop data acquisition mode,[37] in which photoelectrons were used to trigger TOF measurements of ions. The coincident photoions were projected onto dual microchannel plates (MCPs) backed by a phosphor screen (Burle Industries, P43), and the images on the screen were recorded by a TE-cooling CCD detector (Andor, DU934N−BV). Furthermore, the three-dimensional (3D) time-sliced velocity image of a specific ion was recorded directly by applying a pulsed high voltage on MCPs as a mass gate with a variable duration from 60 ns to dc.[38]

To understand dissociative photoionization mechanisms, DFT at the B3LYP/6-311++G(d) level was used to optimize geometries of NO_2 neutral and its cation in their ground states, respectively. Since only two electronically excited states, a^3B_2 and b^3A_2, were paid attention to in this study, the corresponding optimized geometries and harmonic vibrational frequencies were calculated with the time-dependent DFT at the TD-B3LYP/6-311++G(d) level. Based on the optimized geometries of specific ionic states, the adiabatic potential energy surfaces of a^3B_2 and b^3A_2 along the ON−O bond length and the θ(O−N−O) bond angle coordinates were mapped at the same level of theory. In this regard, at every given R(ON−O) bond length and θ(O−N−O) bond angle, the unbroken N−O bond length was reoptimized to verify local minima. Then, a minimum energy path (MEP) on the potential energy surface was plotted, and thus, the adiabatic decomposition mechanism of NO_2^+ in the specific electronic state was readily revealed. All these quantum chemical calculations were performed using the Gaussian 16 A.03 program package.[39]

Additionally, using the optimized geometries, harmonic frequencies, and normal-mode vectors for each electronic state, the Franck−Condon factor (FCF) calculations were conducted as the overlaps between initial and target vibrational states in the harmonic approximation using the ezSpectrum program.[40] Then, the TPE spectrum of NO_2 in a specific electronic state was simulated with a certain full width at half-maximum (fwhm), according to experimental spectra, to assign vibrational progressions of each specific electronic transition from neutral to cation as we did in other systems.[41−44]

3. RESULTS AND DISCUSSION

3.1. Threshold Photoelectron Spectrum of NO_2^+ in the a^3B_2 and b^3A_2 States. TPE spectrum of NO_2 in the energy range of 12.8−14.0 eV was recorded with an increment of 2 meV, and plotted in Figure 1, where the a^3B_2 and b^3A_2 ionic states were both involved. A series of vibrational peaks are clearly observed for each electronic state and summarized in Table 1, where the previous TPE,[16] PFI-ZEKE[18] and photoelectron spectral[12] assignments are listed, too. Our and previous TPE spectra show the very consistent band origins and vibrational structures for these two states, while the PFI-ZEKE and photoelectron spectral results have a slight energy shift by ∼20 meV. Since the weak extraction electric fields (a few to 15 V·cm^{-1}) were used in all these experiments, Stark effect could only lead to a shift of less than 2.5 meV, which is much smaller than those we observed. Therefore, the differences among these measurements, especially in band origins between the TPE spectra and photoelectron spectrum,[12] might be caused by variations of ionization cross section at the He-I radiation and threshold photoionization. In those TPE spectra, the autoionization of Rydberg states nearby probably has non-negligible contributions. Moreover, a

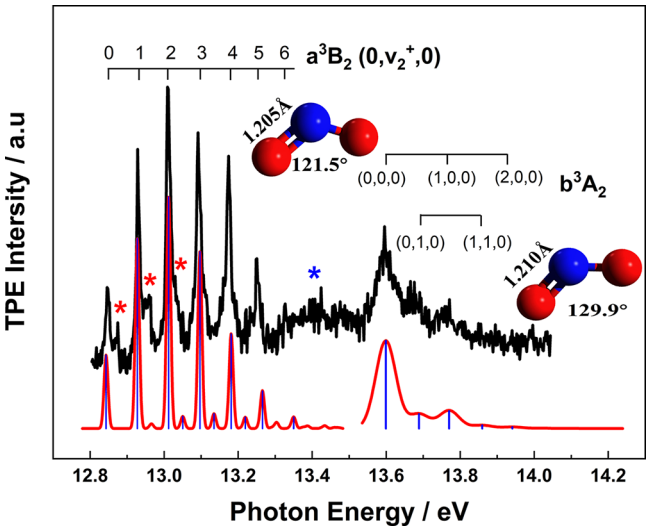

Figure 1. Threshold photoelectron spectrum of NO_2 in the photon energy range of 12.8−14.0 eV, with an increment of 2 meV, where the vibrational progressions are assigned. Franck−Condon simulations were performed for both a^3B_2 and b^3A_2 states at room temperature and plotted with red lines, and the details of the FC model are described in the text. The red and blue asterisk mark the contributions of N_2O_4 photoionization to produce the B^2A_u and C^2B_{1g}/D^2B_{3u} ionic states, respectively.[46]

broadened background (marked with blue star) can be observed at the Franck−Condon gap between these two states in Figure 1. However, no neutral Rydberg states exist in this range,[15] and it has not been observed in the previous He-I photoelectron spectrum[12] either. Consequently, the only reasonable explanation for this background centered at ∼13.4 eV is the contribution of the dimer N_2O_4 photoionization,[45,46] since the thermal population ratio of the dimer is non-negligible at room temperature, about 12% according to a thermal equilibrium of $2NO_2 \leftrightarrow N_2O_4$. According to the recent TPE spectrum of N_2O_4 dimer,[46] the C^2B_{1g} or D^2B_{3u} ionic states of dimer just cover a TPE band here, while the B^2A_u band with sharp features located in the 12.87−13.03 eV range also agrees with those peaks with red asterisks in Figure 1. In fact, the contribution of the dimer ions also can be verified in the following TOF mass spectra.

According to the previous assignments,[12,14,16,18] seven distinct peaks of the first vibrational sequence at 12.842, 12.929, 13.009, 13.092, 13.174, 13.250, and 13.327 eV, are attributed to the a^3B_2 state. In the optimized geometry of $NO_2^+(a^3B_2)$ at the TD-B3LYP level, both N−O bond lengths are 1.205 Å, close to their values (1.193 Å) of the neutral in the ground state, while the bond angle is significantly decreased from 134.4° in the X^2A_1 neutral to 121.5° in the a^3B_2 cation, indicating a bending (ν_2^+) excitation in photoionization. Thus, these seven peaks are readily attributed to the $\nu_2^+ = 0-6$ levels of $NO_2^+(a^3B_2)$. The interval of 78 ± 2 meV (629 cm^{-1}) agrees well with the calculated bending frequency, 660 cm^{-1}. Moreover, the most intense vibrational population is located on $\nu_2^+ = 2$ in the a^3B_2 band (Figure 1), validating a moderate bending from the neutral to NO_2^+ in the a^3B_2 state. To further verify these spectral assignments, the FCF calculation was performed using the DFT optimized geometries and calculated frequencies of $NO_2^+(a^3B_2)$ and the neutral in the ground state. Then, the Franck−Condon simulated line spectrum was convoluted with a Gaussian distribution with a fwhm of 50

https://doi.org/10.1021/acs.jpca.1c00701
J. Phys. Chem. A 2021, 125, 3316−3326

Table 1. Spectral Assignments, Ionization Energies, and Relative Intensities of the Threshold Photoelectron Spectrum of NO_2 in the Photon Energy Range of 12.80−14.0 eV

	ionization energy (eV)				relative intensity	
assignment	present	TPES[16]	PFI-ZEKE[18]	PES[12]	present	PES[12]
$a^3B_2(0,0,0)$	12.842	12.848	12.862	12.8605	24.3	25.5
$a^3B_2(0,1,0)$	12.929	12.928	12.941	12.9396	77.9	76.1
$a^3B_2(0,2,0)$	13.009	13.010	13.020	13.0185	100	100
$a^3B_2(0,3,0)$	13.092	13.092	13.100	13.0971	83.8	77.4
$a^3B_2(0,4,0)$	13.174	–	13.179	13.1750	75.3	41.9
$a^3B_2(0,5,0)$	13.250	–	13.258	13.2523	39.1	17.9
$a^3B_2(0,6,0)$	13.327	–	13.337	13.3258	23.6	7.0
$b^3A_2(0,0,0)$	13.599	–	13.593	13.592	100	100
$b^3A_2(0,1,0)$	13.676	–	13.678	13.677	53.4	41.8
$b^3A_2(1,0,0)$	13.763	–	–	13.762	43.5	37.9

cm^{-1} to account for rotational envelope. A satisfactory agreement between the experimental and FC simulated spectra in Figure 1 validates our above assignments.

For the b^3A_2 state, much broadened vibrational peaks are observed in the TPES of Figure 1, resulting in a serious overlapping and a blurred vibrational structure. Referring to the previous photoelectron spectrum,[12] three vibrational peaks can be distinct, i.e., 13.599, 13.676, and 13.763 eV in Table 1. Similarly, we also performed TD-B3LYP calculations on the geometry and vibrational frequencies of $NO_2^+(b^3A_2)$. At the TD-B3LYP level, both N−O bonds are increased to 1.210 Å, and the bond angle is 129.9°. In comparison to the neutral, the similar geometries imply the 0−0 band of b^3A_2 should be the most intense, and both symmetric stretching (ν_1^+) and bending (ν_2^+) modes could be excited in photoionization. As shown in Figure 1, the Franck−Condon simulation with a fwhm of 250 cm^{-1} validates our predictions. The vibrational frequencies are determined to be 1274 and 630 cm^{-1}, and generally consistent with the TD-B3LYP frequencies.

3.2. TPEPICO Time-of-Flight Mass Spectra. Figure 2 shows the five representative TPEPICO time-of-flight (TOF) mass spectra for the dissociative photoionization of NO_2, *e.g.* 12.929, 13.009, 13.092, and 13.174 eV for $a^3B_2(0,\nu_2^+=1-4,0)$, and 13.599 eV for $b^3A_2(0,0,0)$ levels. Since only the $NO^+(X^1\Sigma^+) + O(^3P_g)$ dissociation limit can be reached in these photon energies, two ions, NO^+ and NO_2^+, are distinctly observed in Figure 2, and their relative intensities are very similar to the previous results.[13] At 12.929 eV for $a^3B_2(0,1,0)$, no NO^+ fragment is observed although the photon energy is beyond the dissociation limit, implying a barrier toward decomposition. The fwhm of the NO_2^+ TOF profile is narrow as 17 ns. When the photon energy reaches 13.009 eV of the $a^3B_2(0,2,0)$ level, an asymmetrical TOF distribution is clearly recorded for NO^+ fragment ions, as well as a part of residual NO_2^+ ions, indicative of a metastable dissociation. Due to a relatively low extraction field (~15 V/cm) in our experiment, ion residence time in the acceleration region is several microseconds, and thus a metastable dissociation leads to an asymmetrical shape of daughter ion peak[47] herein. In this regard, such the asymmetrical TOF profile indicates the dissociation rate constant at this energy is ca. 10^6 s^{-1} under the present experimental conditions. Moreover, as the photon energy increases to or beyond $a^3B_2(0,3,0)$, the NO^+ TOF profile becomes symmetric owing to the faster dissociation. As shown in Figure 2, the TOF distribution of NO^+ is broadened to more than 400 ns (fwhm) due to a great deal of released kinetic energy in dissociation. All these evidence strongly suggest that there is a relatively deep potential well of a^3B_2 along the N−O bond, which is consistent with the previous studies.[5,19] Moreover, the triangle-like TOF distribution of NO^+ in Figure 2 is different from the reported anisotropic profiles in the Eland and Karlsson's PEPICO experiment,[13] but it is consistent with the recent imaging PEPICO measurements.[17,33]

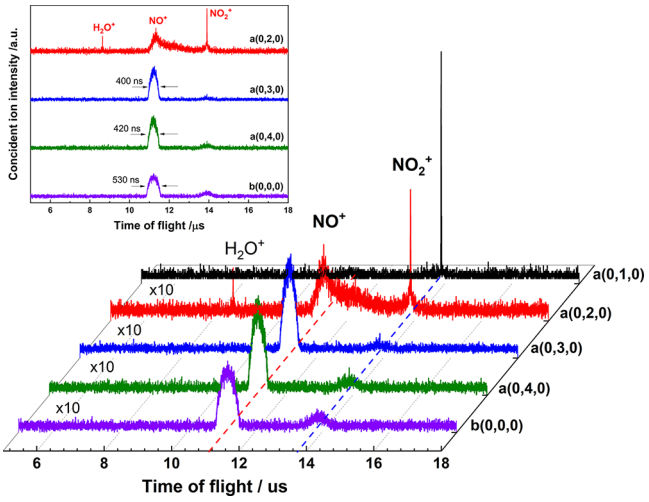

Figure 2. TPEPICO TOF mass spectra for vibrational state-selected dissociative photoionization of NO_2 via the a^3B_2 and b^3A_2 states, in which the $a^3B_2(0,\nu_2^+=1-4,0)$ and $b^3A_2(0,0,0)$ ionic states were recorded at 12.929, 13.009, 13.092, 13.174, and 13.599 eV, respectively.

To our surprise, a very wide NO_2^+ ion peak was still observed at the higher energies like $a^3B_2(0,4,0)$ and $b^3A_2(0,0,0)$ in Figure 2. Apparently, its TOF distribution such as the width and profile is entirely different from that from direct photoionization of NO_2 monomer (black trace in Figure 2). According to thermal equilibrium between NO_2 monomer and N_2O_4 dimer at room temperature, the photoionization of the dimer is involved in our experiment as well, as observed in the TPES of Figure 1. Due to the fast decomposition of the $N_2O_4^+$ dimer ion in the present photon energy range, we could not observe the $N_2O_4^+$ dimer parent ion in TOF mass spectra, and only the NO_2^+ fragment ion was residual in Figure 2, with a broadened TOF distribution due to the released kinetic energy in decomposition.

3.3. TPEPICO Image of NO^+ Dissociated from $NO_2^+(a^3B_2)$. Although the kinetic energy released distributions

https://doi.org/10.1021/acs.jpca.1c00701
J. Phys. Chem. A 2021, 125, 3316−3326

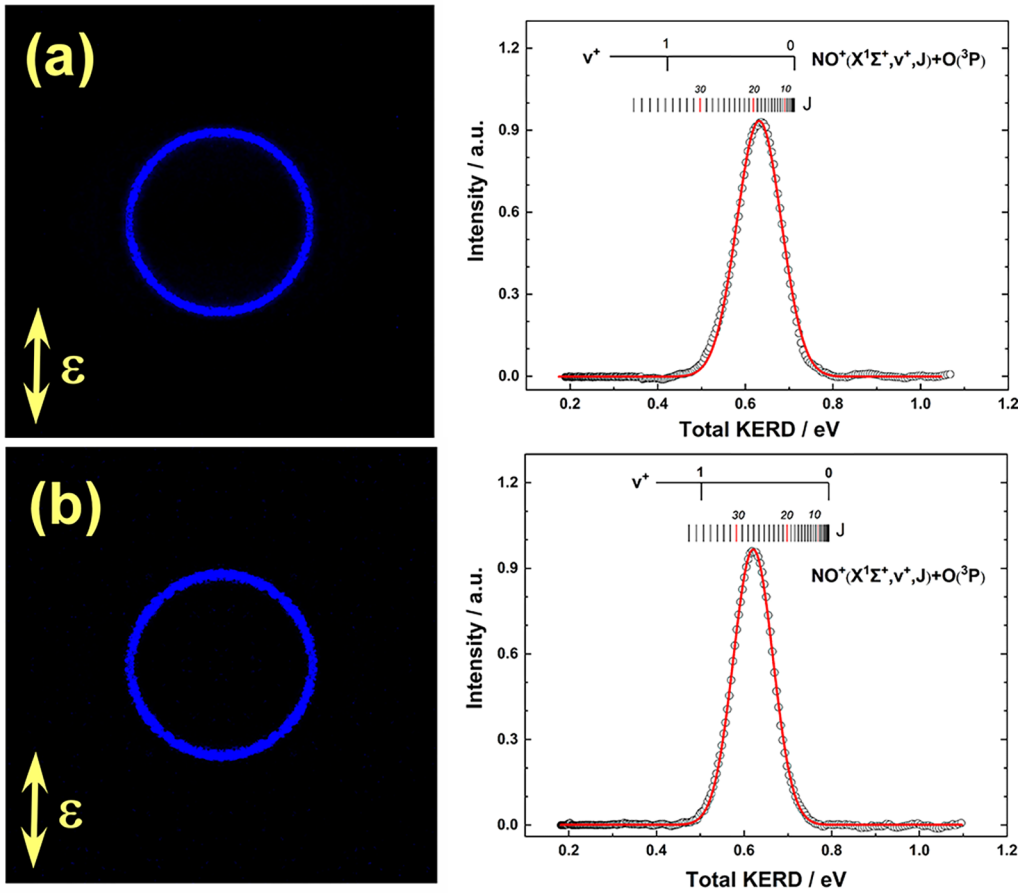

Figure 3. Time-sliced TPEPICO velocity map images of NO^+ and the correspodning total kinetic energy released distributions, recorded at (a) 13.092 eV for $a^3B_2(0,3,0)$ and (b) 13.174 eV for $a^3B_2(0,4,0)$, respectively. The polarization of electric vector ε of VUV photons is vertical in the images, and the fitted total KERD curves with a Gaussian profile are plotted with the red solid lines.

Table 2. Available Energy (E_{ava}), Kinetic Energies, and Ro-vibrational Energies (E_{vr}) of Fragments, Mean Total Kinetic Energy ($\langle E_T \rangle$) in the Dissociation of NO_2^+ in the $a^3B_2(0,3,0)$, $a^3B_2(0,4,0)$, and $b^3A_2(0,0,0)$ States, as Well as the Corresponding Anisotropy Parameters (β)

		kinetic energy (eV)					
vibronic levels	E_{ava} (eV)	$NO^+(^1\Sigma^+)$	$O(^3P_g)$	$\langle E_T \rangle$	f_T[a]	E_{vr} (eV)	β
$a^3B_2(0,3,0)$	0.712	0.220	0.413	0.633	0.88	0.089	0.14 ± 0.1
$a^3B_2(0,4,0)$	0.794	0.215	0.315	0.619	0.78	0.179	0.13 ± 0.1
$b^3A_2(0,0,0)$	1.219	0.253[b]	0.474	0.895	0.73	0.324	0.15 ± 0.1
		0.341[c]	0.638				0.05 ± 0.1

[a] $f_T = \langle E_T \rangle / E_{ava}$, which is the proportion of mean total kinetic energy $\langle E_T \rangle$ to available energy E_{ava}. [b] For the channel to produce $NO^+(^1\Sigma^+,v^+=1)$ from NO_2^+ in $b^3A_2(0,0,0)$. [c] For the channel to produce $NO^+(^1\Sigma^+,v^+=0)$ from NO_2^+ in $b^3A_2(0,0,0)$.

of fragment ions can be roughly derived from fitting the corresponding TOF profiles,[48−52] the detailed ro-vibrational distributions are difficult to be discerned in this respect. Moreover, the angular distributions in dissociation cannot be obtained either. Therefore, in order to clearly uncover the excess energy distribution in the dissociation of NO_2^+ ions in the a^3B_2 and b^3A_2 states, the TPEPICO velocity image of NO^+, the unique fragment ion, was recorded. Thanks to the special ion optics in our TPEPICO imaging spectrometer, a relatively high energy resolution ($\Delta E_T/E_T \sim 3\%$)[34] was achieved for ion imaging. Thus, accurate KERDs and angular distributions were obtained simultaneously.

Based on the TOF mass spectra in Figure 2, the symmetrical TOF distribution of NO^+ was observed when the photon energy reached the $a^3B_2(0,3,0)$ level, and thus three-dimensional time-sliced TPEPICO velocity image of NO^+ was recorded at two representative photon energies, 13.092 eV for $a^3B_2(0,3,0)$ and 13.174 eV for $a^3B_2(0,4,0)$, respectively, using a mass gate of 60 ns. Although the false coincidence events have been significantly reduced due to the specially designed electric field,[34] the residual contributions still exist in all recorded images. Moreover, according to the perpendicular configuration between the molecular beam (MB) and the ion flight direction, the velocity spread of MB contaminates images along its direction. Consequently, a multistep data reduction process of subtracting, deconvolution, and quadrant symmetrization is necessary to obtain the better-resolution velocity map images.[53−55]

Figure 3 shows the modified TPEPICO velocity images of NO^+ at 13.092 and 13.174 eV, as well as the corresponding

https://doi.org/10.1021/acs.jpca.1c00701
J. Phys. Chem. A 2021, 125, 3316−3326

total KERDs, based on the conservation of energy and momentum in dissociation. A sole ring is observed in each image, and every total KERD curve is perfectly fitted with a Gaussian profile as shown in the red line of Figure 3. For dissociation of NO_2^+ in the $a^3B_2(0,3,0)$ and $a^3B_2(0,4,0)$ states, both dominant total KERDs are located at ca. 0.62 eV, spanning from 0.5 to 0.75 eV. The kinetic energy of the NO^+ fragment ion and the total KERDs are summarized in Table 2, together with the available energy relative to the dissociation limit. Moreover, no obviously anisotropic distribution is observed in the images of Figure 3 either. By integrating the image intensities over a proper radius range of speed at each angle, the angular distribution of NO^+ fragment ion, $I(\theta)$, was obtained, and then the anisotropy parameter β for a specific dissociation channel was derived from fitting $I(\theta)$ with the formula, $I(\theta) = (4\pi)^{-1}\cdot[1 + \beta\cdot P_2(\cos\theta)]$, where θ is the angle between the recoil velocity of fragments and the polarization of electric field vector ε of VUV photons, and $P_2(\cos\theta)$ is the second-order Legendre polynomial. As listed in Table 2, the β values were both close to zero for the dissociation of NO_2^+ in the $a^3B_2(0,3,0)$ or $(0,4,0)$ states, indicating that the bond breaking of a^3B_2 state occurs in a larger time scale than the period of molecular rotation indeed.

Taking the dissociation limit D_0 = 12.3797 eV for $NO^+(X^1\Sigma^+)$ + $O(^3P)$, as well as the spectroscopic parameters of NO^+, such as the vibrational frequency ν^+ = 2376.42 cm^{-1},[56] the anharmonicity parameter ω_eX_e = 16.262 cm^{-1}, and the rotational constants B_e = 1.997 cm^{-1},[57] the ro-vibrational energy levels of NO^+ fragment ion are calculated and marked in the total KERD curves of Figure 3. Apparently, the NO^+ fragment ion dissociated from NO_2^+ in $a^3B_2(0,3,0)$ has a "cold" vibrational (ν^+ = 0) and "hot" rotational (J = 0−28) population, with a center at J = 19, which is greatly consistent with Tang et al.'s recent observation that the ro-vibrational state of NO^+ is dominantly populated at ν^+ = 0 and J = 21.[17] For the dissociation of NO_2^+ at $a^3B_2(0,4,0)$, the dominantly ro-vibrational population of $NO^+(X^1\Sigma^+)$ is located at ν^+ = 0 and J = 18−33, with a center of J = 27. Therefore, a correlation between internal state populations of parent and fragment can be summed up for $NO_2^+(a^3B_2)$, that the increase in bending vibrational amplitude of NO_2^+ directly leads to an enhanced rotation of NO^+ fragment ion. The same conclusion was also obtained by Tang et al. based on their imaging PEPICO measurement.[17] In fact, such a "cold" vibrational and "hot" rotational population of NO^+ strongly indicates that the molecular geometry of NO_2^+ keeps bent just prior to dissociation.

For dissociation of a triatomic molecule, the classical impulsive model[58] has usually been used to estimate energy distributions of fragments in a direct dissociation along a repulsive potential energy surface, in which the third atom plays a spectator role when bond breaking rapidly occurs. In this case, the proportion of the mean total kinetic energy $\langle E_T\rangle$ to the available energy (E_{ava}) can be calculated as the following equation , eq 1 for dissociation of NO_2^+,

$$f_T = \frac{\langle E_T\rangle}{E_{ava}} = \frac{\mu_{O-N}}{\mu_{O-NO}} = 0.72 \quad (1)$$

where μ is the reduced mass. As indicated in Table 2, the f_T values are experimentally determined to be 0.88 for $a^3B_2(0,3,0)$ and 0.78 for $a^3B_2(0,4,0)$, respectively. Apparently, these data are generally close to the theoretical limit, indicating that the ON−O bond breaking occurs along a potential energy surface with repulsive characteristics, instead of a statistical decomposition process.

3.4. O-Loss Mechanism in the Dissociation of NO_2^+ in the a^3B_2 State. As mentioned above, there are some controversies about the dissociation mechanism of $NO_2^+(a^3B_2)$ ions in previous experimental and theoretical studies.[13,16,17,19] In the photoelectron spectroscopy[13,16] and PEPICO[17] experiments, some possible mechanisms were proposed for the a^3B_2 dissociation, such as the tunneling, the avoided crossing between two $^3B_2$ states,[13] the intersystem crossing,[16] and the coupling between the a^3B_2 state and the upper 2^3B_1 ionic state.[17] However, the high-level CASPT2 calculations by Chang and Huang[19] were opposed to these deductions. Based on the barrier height of 0.42 eV, an adiabatic ON−O bond rupture was proposed for the a^3B_2 state by them, i.e., a vibrational predissociation to overcome such a low barrier in ON−O stretching coordinate.[19]

To reveal the true ON−O bond rupture mechanism of $NO_2^+(a^3B_2)$, a whole potential energy surface including bending and N−O stretching coordinates is necessary. According to the previous calculations,[11,12] the first dissociation limit of $NO^+(X^1\Sigma^+)$ + $O(^3P)$ adiabatically correlates with the a^3B_2, b^3A_2, and $2^3A''$ states, while the $X^1\Sigma_g^+$, A^1A_2, and B^1B_2 states link adiabatically to the second dissociation limit of $NO^+(X^1\Sigma^+)$ + $O(^1D)$. Thus, we only performed the TD-B3LYP calculations to map potential energy surfaces of a few low-lying electronic states, *e.g.*, $X^1\Sigma_g^+$, a^3B_2 and b^3A_2. Figure 4 shows the calculated adiabatic potential energy surface of a^3B_2 along the ON−O bond length and θ(O−N−O) bond angle coordinates.

As shown by the minimum energy path (MEP) in Figure 4 (black trace), the fragmentation observed in experiments is just an adiabatic ON−O bond rupture process. $NO_2^+(a^3B_2)$ has a local minimum near Franck−Condon region on the potential energy surface with a barrier. The calculated barrier height is only 0.41 eV at the TD-B3LYP/6-311++G(d) level, which

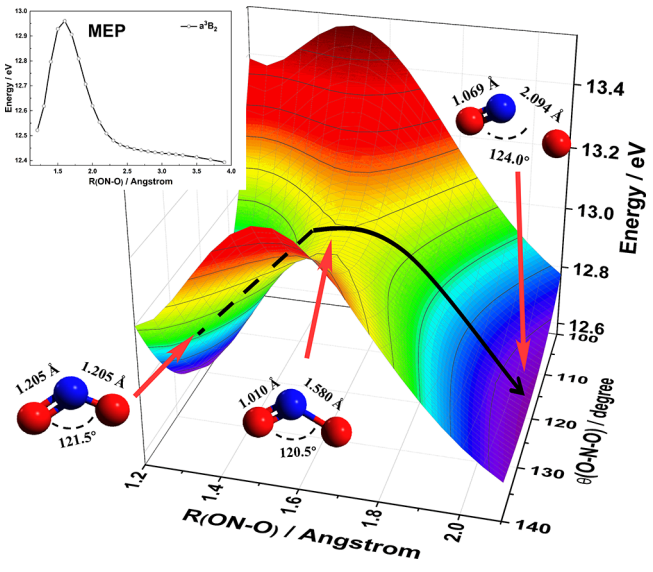

Figure 4. Adiabatic potential energy surface of NO_2^+ in the a^3B_2 state, calculated at the TD-B3LYP/6-311++G(d) level, along the ON−O bond rupture and bond angle θ(O−N−O). The minimum energy path (MEP) is shown with the black curve, and it is also plotted in the inserted panel.

https://doi.org/10.1021/acs.jpca.1c00701
J. Phys. Chem. A 2021, 125, 3316−3326

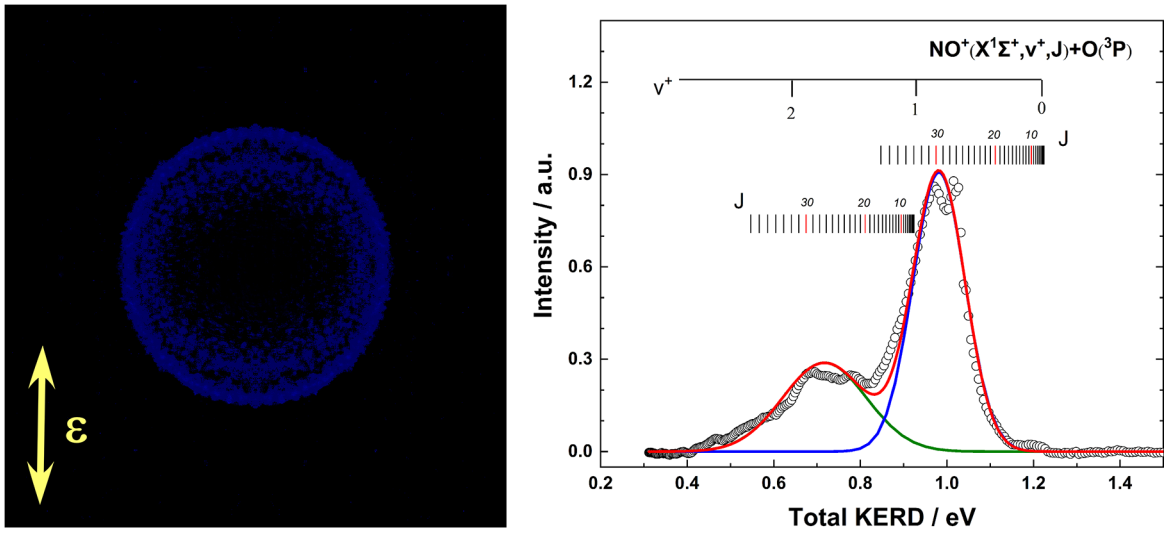

Figure 5. Time-sliced TPEPICO velocity map image of NO^+ and the correspodning total kinetic energy released distribution, recorded at 13.599 eV for $b^3A_2(0,0,0)$. The polarization of electric vector ε of VUV photons is vertical in the images, and the fitted total KERD curve in a red solid line is plotted as a sum of two Gaussian profiles in color dashed lines.

agrees very well with the CASPT2 result (0.42 eV).[19] Such the energy agreement clearly indicates that no significant multi-configuration interaction exists for the a^3B_2 state, which can also be confirmed by the Chang and Huang's CASSCF wave function analyses on electronic configuration.[19] Actually, a lower barrier height of 0.32 eV was obtained in a higher-level CBS-QB3 calculation with zero-point energy correction, which is closer to the experimental onset (0.25 eV, as the energy difference between the (0,0,0) and (0,3,0) levels). That is to say, the barrier height might be overestimated in previous calculations.[5,19] Moreover, the unbroken N−O bond is slightly shortened along this MEP from 1.205 Å in $NO_2^+(a^3B_2)$ to 1.010 Å in the transition state and to 1.069 Å in the NO^+ fragment ion, as shown in Figure 4. Meanwhile, the θ(O−N−O) bond angle slightly increases. Although the MEP shown in Figure 4 is only extended to the ON−O bond length of 2.1 Å, far from the asymptote products, the molecular geometry of NO_2^+ ion is certainly maintained as a bending structure prior to dissociation. In this case, the recoil momentum naturally results in large rotation of NO^+ fragment ion, when the ON−O bond is rapidly broken at this bent structure. Moreover, NO^+ is kept in the vibrational ground state because the excess energy distributed on vibrational degree of freedom in the impulsive dissociation approximation is only 0.06 eV as $E_v = E_{a\nu a}(1 - f_T)\cdot\cos^2\theta$, where θ is the bond angle at the exit, for example, θ = 124° for a^3B_2, and is apparently not enough for NO^+ vibrational excitation. Therefore, based on our MEP calculation we can perfectly explain our experimentally ro-vibrational distributions of NO^+ dissociated from NO_2^+ ion in the a^3B_2 state. Additionally, the imaginary vibrational frequency of the transition state was calculated to be only 568 cm^{-1} at the TD-B3LYP/6-311++G(d) level. Such a small value indicates that the tunneling effect suggested by Eland and Karlsson[13] is ignored, which agrees with the common sense about an insignificant tunneling for those fragments of heavy mass. Furthermore, our calculation also shows that no obvious interaction from the upper electronic states of $^3B_2$ or $^3B_1$ is found along the MEP. Thus, the avoided crossing between two $^3B_2$ states[13] and the coupling between a^3B_2 and 2^3B_1 states[17] do not exist or are negligible in the a^3B_2 dissociation. As calculated in Chang and Huang's CASSCF calculations,[19] a relatively strong spin−orbit coupling only exists between $X^1\Sigma_g^+$ and a^3B_2. That is to say, the intersystem crossing mechanism[16] is not trustworthy either. Therefore, based on the excellent agreement between the MEP calculation and TPEPICO imaging experiments, an adiabatic ON−O bond breaking mechanism can be validated for the vibrational predissociation of $NO_2^+(a^3B_2)$, i.e., the vibrationally excited NO_2^+ cation overcomes the adiabatic barrier along the ON−O rupture coordinate, and dissociates toward NO^+ and oxygen atom at a bent geometry. Additionally, unlike usual vibrational predissociations, the nonstatistical KERD is found for the $NO_2^+(a^3B_2)$ decomposition, and its $\langle f_T \rangle$ value is close to that of the "impulsive" model, indicating that the N−O bond breaking rapidly occurs to keep the other oxygen atom as a spectator on the exit potential energy surface.

3.5. N−O Bond Rupture Mechanism of $NO_2^+(b^3A_2)$.

Figure 5 shows the modified TPEPICO velocity images of NO^+ at 13.599 eV, as well as the corresponding total KERDs, where the NO_2^+ ions were prepared in the $b^3A_2(0,0,0)$ state. Due to the weak intensities of vibrational excited states in TPE spectrum of Figure 1, we failed to record TPEPICO images for those vibronic levels except for (0,0,0). Although the photon energy is slightly increased from a^3B_2, the images of NO^+ exhibit a significant change, that there are two rings with different diameters observed clearly, and the outer one is brighter. Since only the lowest dissociation limit of $NO^+(X^1\Sigma^+) + O(^3P)$ is open at this photon energy, these rings naturally imply the formation of vibrationally excited NO^+ fragment ions.

Similar to the internal energy assignments of Figure 3, the ro-vibrational energy levels of the NO^+ fragment ion are calculated, too, with considering the dissociation limit and the spectroscopic parameters of NO^+. The vibronic levels are noted in the total KERD curve of Figure 5. To our surprise, the NO^+ fragment ion dissociated from NO_2^+ in $b^3A_2(0,0,0)$ typically shows a very "hot" rotational distribution ($J \sim 30$) and a certain vibrationally excited ($v^+ = 0-1$) populations, which is apparently different from that of the a^3B_2 dissociation in Figure 3. Moreover, the vibrationally excited ($v^+ = 1$)

https://doi.org/10.1021/acs.jpca.1c00701
J. Phys. Chem. A 2021, 125, 3316−3326

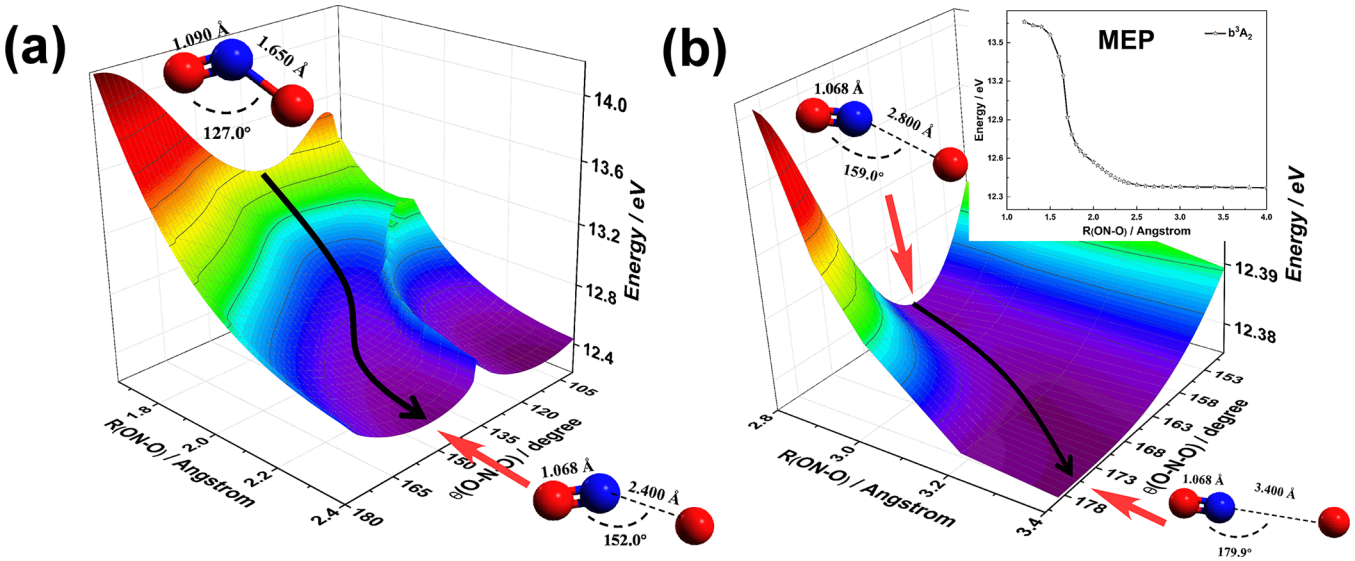

Figure 6. Adiabatic potential energy surface of NO_2^+ in the b^3A_2 state, calculated at the TD-B3LYP/6-311++G(d) level, along the ON−O bond rupture and bond angle θ(O−N−O), (a) R(ON−O) = 1.65−2.40 Å and (b) R(ON−O) = 2.80−3.40 Å. The minimum energy path (MEP) is shown with the black curve, and it is also plotted in the inserted panel.

population (corresponding to the inner ring) accounts for approximately about 28% of the total NO^+ fragment ions. It is worth noting that the present internal energy populations are somewhat different from the Tang et al.'s imaging PEPICO conclusions,[17] in which a sole vibrational (v^+=0) population with high and wide J rotational excitation (extending to the v^+=1 population) was observed for NO^+ fragment ions dissociated from NO_2^+ in the $b^3A_2(0,0,0)$ state. Thanks to the higher energy resolution of our TPEPICO imaging,[34] this wide distribution observed by Tang et al. is split to two vibrational components (v^+ = 0 and 1). Therefore, our experiment provides a more detailed and reliable population of NO^+ fragment ion, and it exhibits more distinct energy distributions in dissociation of a^3B_2 and b^3A_2 states.

As listed in Table 2, the anisotropy parameters for these two vibrational channels are 0.05 ± 0.1 for $NO^+(X^1\Sigma^+,v^+=0)$ and 0.15 ± 0.1 for $NO^+(X^1\Sigma^+,v^+=1)$, respectively, by fitting the angular distribution of NO^+ at a specific speed range in the image. For the NO_2^+ triatomic molecule, the transition dipole moment to produce the b^3A_2 state is perpendicular to the plane of the molecule.[32] Thus, the photon mainly ionizes molecules that lie in a plane perpendicular to the polarization of the electric field vector. Since the recoil of oxygen atom and NO^+ fragment proceeds in-plane, the near zero β value in Table 2 decisively indicates the bond breaking occurs on a time scale which is larger than overall rotation of parent molecule. From another point of view, the $b^3A_2(0,0,0)$ state does not show a typically fast dissociation characteristic along a repulsive potential energy surface, providing an additional evidence of the quasi-minimum property for the b^3A_2 state with a very shallow well (less than 0.1 eV) in the Franck−Condon region, as calculated in previous multireference configuration interaction (MRCI) calculations.[5] In principle, a more anisotropic distribution can be predicted for dissociation of a vibrationally excited state like $b^3A_2(1,0,0)$. However, due to too weak intensities of these vibrationally excited states in TPES of Figure 1, the TPEPICO velocity imaging cannot be performed regretfully.

In comparison to the "cold" vibrational population of NO^+ produced from $NO_2^+(a^3B_2)$ cation, the dissociation of $b^3A_2(0,0,0)$ state shows different ro-vibrational population as both "hot" rotation and vibration, although the $a^3B_2(0,3,0)$ and $a^3B_2(0,4,0)$ levels are also beyond the dissociation limit of $NO^+(X^1\Sigma^+,v^+=1)$ + $O(^3P)$. Therefore, the ON−O bond rupture mechanism of NO_2^+ in the b^3A_2 state should be different from that of a^3B_2. In fact, a relatively consistent mechanism of the b^3A_2 dissociation has been proposed before,[13,16,17,19] that a direct ON−O bond rupture occurs on its adiabatic potential energy surface. Consequently, the TD-B3LYP calculation was performed to map its adiabatic potential energy surface, especially along bending and N−O stretching coordinates, to uncover potential reasons for different internal energy distributions of NO^+ dissociated from NO_2^+ in the a^3B_2 and b^3A_2 states.

For simplicity, the adiabatic potential energy surface after the barrier is plotted in Figure 6, i.e., R(ON−O) from 1.65 to 3.40 Å. Compared with the optimized geometry of $NO_2^+(b^3A_2)$ in Figure 1, the unbroken N−O bond length is shortened to 1.090 Å, and the bond angle is slightly reduced to 127.0° at the beginning point of Figure 6, R(ON−O) = 1.65 Å. As shown by the MEP in the black trace of Figure 6, the greatest repulsive force is located at the initial stage, i.e., R(N−O) is from 1.5 to 1.8 Å, in which the bond angle is almost unchanged. However, a typical curve crossing by an upper $2^3B_1(3^3A'')$ state is confirmed at R(N−O) ~ 2.0 Å (Figure 6a), which builds a potential wall to hinder the direct bond rupture and drive the bending of molecule to a quasi-linear configuration as shown in the distorted MEP in Figure 6. Thus, a classical impulsive dissociation is disturbed by this interaction after R(N−O)=2.0 Å, slowing the departure of the oxygen atom. As a result, near the exit potential energy surface the recoil momentum in the quasi-linear $[ON\cdots O]^+$ complex prefers to enhance the NO^+ vibration. In other words, although most excess energy is released into translation degree of freedom at the initial decomposition stage, the exit potential energy surface with a quasi-linear structure plays a considerable role to redistribute the NO^+ ro-vibrational population in some

https://doi.org/10.1021/acs.jpca.1c00701
J. Phys. Chem. A 2021, 125, 3316−3326

extent, and hence more excess energy than the predicted value by the classical impulsive model is distributed on the vibrational degree of freedom under the action of recoil momentum. It is worth noting that the excess energy distributed on vibrational degree of freedom following the impulsive approximation can be calculated to be ca. 0.16 eV for b^3A_2, when fixing the bond angle at 130°. Apparently, this energy is not enough for the NO^+ vibrational excitation, too, and is opposite to our experimental observation. However, given the quasi-linear configuration on the exit, this vibrationally distributed energy in the impulsive approximation will be increased to 0.34 eV, larger than the energy limit to produce $NO^+(v^+=1)$. This well demonstrates that the interaction from the upper $2^3B_1(3^3A'')$ state still has a significant influence on such a direct dissociation along repulsive potential energy surface.

In addition, this quasi-linear structure at the exit potential energy surface disagrees with Toffoli et al.'s conclusion,[32] that the recoil angle was ∼120° in dissociation of NO_2^+ in the b^3A_2 state. We would like to emphasize that in Toffoli et al.'s experiment,[32] dissociative photoionization of NO_2 via b^3A_2 was induced by a photon of 14.4 eV, while that of our measurement was located near the threshold of b^3A_2 (13.599 eV). This means that the vibrational excited $NO_2^+(b^3A_2)$ ion was produced by Toffoli et al., and was different from the $b^3A_2(0,0,0)$ state in current study. Furthermore, vibrational energy in Toffoli et al.'s experiment is higher than the ring-shape barrier height in the b^3A_2 potential energy surface of Figure 6a, and hence, its dissociation occurs directly along bond breaking with a faster rate and a larger β value.

4. CONCLUSIONS

Using the TPEPICO velocity imaging approach coupled to VUV photoionization at the Hefei Light Source, the dissociative photoionization of NO_2 in the photon energy range of 12.8−14.0 eV has been investigated thoroughly. Both a^3B_2 and b^3A_2 states of NO_2^+ were prepared with fine vibrational structures in this energy range. The great agreements were obtained with previous results for spectral assignments for the vibrational progresses of these two electronic states. Moreover, both NO_2^+ and NO^+ ions were observed in the TPEPICO TOF mass spectra at the a^3B_2 and b^3A_2 states, except for the $a^3B_2(0,0,0)$ and $a^3B_2(0,1,0)$ levels. Specially, the TOF distribution of NO^+ was changed from an asymmetrical peak at $a^3B_2(0,2,0)$ to a broadened symmetric profile at higher vibronic levels. This vibrationally dependent dissociation behavior strongly indicates the predissociative property of a^3B_2, which agrees with theoretical calculations.

To address the previous dispute about the $NO_2^+(a^3B_2)$ dissociation mechanism, the 3D time-sliced TPEPICO velocity images of NO^+ as the unique fragment ion were recorded at the $a^3B_2(0,3,0)$ and $a^3B_2(0,4,0)$ levels. Then, the kinetic energy release, ro-vibrational population and angular distribution of NO^+ were achieved. Interestingly, a typical "cold" vibrational ($v^+ = 0$) and "hot" rotational population is obtained, while the $\langle f_T \rangle$ values are close to the "impulsive" dissociation limit. According to the MEP on potential energy surface at the TD-B3LYP level, a adiabatic ON−O bond breaking mechanism is validated for the vibrational predissociation of $NO_2^+(a^3B_2)$. In this relatively slow NO_2^+ decomposition process, an "impulsive" dissociation model plays an important role after overcoming the barrier toward NO^+ and oxygen atom, in which the parent cation maintains a bent geometry. Similarly, the TPEPICO velocity imaging and the TD-B3LYP calculations were conducted for the dissociation of NO_2^+ in the $b^3A_2(0,0,0)$ state. The quasi-linear geometry of the parent cation on the exit of adiabatic potential energy surface provides an additional force to enhance vibrational excitation of NO^+ fragment ion, leading to both "hot" vibrational and rotational populations.

Additionally, the agreement between the experimental and theoretical $\langle f_T \rangle$ values of the classical "impulsive" model has always been used to judge if the dissociation occurs on a repulsive potential energy surface.[42,53−55,59,60] However, the dissociation of NO_2^+ in the a^3B_2 and b^3A_2 states provides an atypical example of a slow "impulsive" dissociation process. Thus, this study provides valuable insights into the application of the classical "impulsive" model on an overall slow dissociation process of a polyatomic molecule.

AUTHOR INFORMATION

Corresponding Authors

Xiaoguo Zhou − *Hefei National Laboratory for Physical Sciences at the Microscale, Department of Chemical Physics, University of Science and Technology of China, Hefei 230026, China*; orcid.org/0000-0002-0264-0146; Email: xzhou@ustc.edu.cn

Shilin Liu − *Hefei National Laboratory for Physical Sciences at the Microscale, Department of Chemical Physics, University of Science and Technology of China, Hefei 230026, China*; Email: slliu@ustc.edu.cn

Authors

Tongpo Yu − *Hefei National Laboratory for Physical Sciences at the Microscale, Department of Chemical Physics, University of Science and Technology of China, Hefei 230026, China*

Xiangkun Wu − *Hefei National Laboratory for Physical Sciences at the Microscale, Department of Chemical Physics, University of Science and Technology of China, Hefei 230026, China*

Xiaohan Ning − *Hefei National Laboratory for Physical Sciences at the Microscale, Department of Chemical Physics, University of Science and Technology of China, Hefei 230026, China*

Yan Chen − *Hefei National Laboratory for Physical Sciences at the Microscale, Department of Chemical Physics, University of Science and Technology of China, Hefei 230026, China; National Institute of Metrology, Beijing 100013, China*

Xinhua Dai − *National Institute of Metrology, Beijing 100013, China*

Fuyi Liu − *National Synchrotron Radiation Laboratory, University of Science and Technology of China, Hefei, Anhui 230029, China*

Complete contact information is available at: https://pubs.acs.org/10.1021/acs.jpca.1c00701

Notes

The authors declare no competing financial interest.

ACKNOWLEDGMENTS

The authors sincerely appreciate Prof. Cheuk Yiu Ng for his fruitful discussions and suggestions on the design of the TPEPICO imaging setup at the National Synchrotron Radiation Laboratory at Hefei, China. The work was financially

supported by the National Key Research and Development program of China (No. 2016YFF0200502), and the National Natural Science Foundation of China (Nos. 21873089, 21903079, and 22073088). X.Z. is also grateful for the funding support of USTC-NSRL Association.

REFERENCES

(1) Lee, T. J.; Rice, J. E. Ab initio study of the molecular structure and vibrational spectrum of nitric acid and its protonated forms. *J. Phys. Chem.* **1992**, *96*, 650−657.
(2) Lee, T. J. Bond distance and vibrational spectrum of the molecular cation NO_2^+. *Chem. Phys. Lett.* **1992**, *188*, 154−158.
(3) Wayne, R. P. *Chemistry of Atmospheres*; Clarendon Press: Oxford, U.K., 1985.
(4) Flesch, G. D.; Ng, C. Y. A study of the reaction $O^+(^4S)+N_2$ using the tandem photoionization mass spectrometric method. *J. Chem. Phys.* **1990**, *92*, 3235−3236.
(5) Hirst, D. M. Ab initio potential energy surfaces for excited states of the NO_2^+ molecular ion and for the reaction of N^+ with O_2. *J. Chem. Phys.* **2001**, *115*, 9320−9330.
(6) Albritton, D. L.; Viggiano, A. A.; Dotan, I.; Fehsenfeld, F. C. Production of $NO^+(a^3\Sigma^+)$ ions in the reaction of N^+ ions with O_2 at 300 K. *J. Chem. Phys.* **1979**, *71*, 3295−3298.
(7) Howorka, F.; Dotan, I.; Fehsenfeld, F. C.; Albritton, D. L. Kinetic energy dependence of the branching ratios of the reaction of N^+ ions with O_2. *J. Chem. Phys.* **1980**, *73*, 758−764.
(8) Guettler, R. D.; Jones, G. C.; Posey, L. A.; Kirchner, N. J.; Keller, B. A.; Zare, R. N. Guided ion beam measurement of the product branching ratios for the ion−molecule reaction $N^+ + O_2$ as a function of collision energy. *J. Chem. Phys.* **1994**, *101*, 3763−3771.
(9) Tully, J. C.; Herman, Z.; Wolfgang, R. Crossed-beam study of the reaction $N^+ + O_2 \rightarrow NO^+ + O$. *J. Chem. Phys.* **1971**, *54*, 1730−1737.
(10) Smith, M. A.; Bierbaum, V. M.; Leone, S. R. Infrared Chemiluminescence from vibrationally excited NO^+ product branching in the $N^+ + O_2$ ion molecule reaction. *Chem. Phys. Lett.* **1983**, *94*, 398−403.
(11) Dalgarno, A.; Fox, J. L. Ion Chemistry in Atmospheric and Astrophysical Plasmas. In *Unimolecular and Bimolecular Ion−molecule Reaction Dynamics*; Ng, C. Y., Baer, T., Powis, I., Eds.; Wiley, Chichester, U.K., 1994; pp 1−86.
(12) Baltzer, P.; Karlsson, L.; Wannberg, B.; Holland, D. M. P.; MacDonald, M. A.; Hayes, M. A.; Eland, J. H. D. An experimental study of the valence shell photoelectron spectrum of the NO_2 molecule. *Chem. Phys.* **1998**, *237*, 451−470.
(13) Eland, J. H. D.; Karlsson, L. Dissociative photoionisation of NO_2 up to 26 eV. *Chem. Phys.* **1998**, *237*, 139−148.
(14) Brundle, C. R.; Neumann, D.; Price, W. C.; Evans, D.; Potts, A. W.; Streets, D. G. Electronic structure of NO_2 studied by photoelectron and Vacuum-UV spectroscopy and Gaussian orbital calculations. *J. Chem. Phys.* **1970**, *53*, 705−715.
(15) Edqvist, O.; Lindholm, E.; Selin, L. E.; Asbrink, L.; Kuyatt, C. E.; Mielczarek, S. R.; Simpson, J. A.; Fischer-Hjalmars, I. Rydberg series of small molecules. VIII. Photoelectron spectroscopy and electron spectroscopy of NO_2. *Phys. Scr.* **1970**, *1*, 172−178.
(16) Shibuya, K.; Suzuki, S.; Imamura, T.; Koyano, I. Dissociation of state-selected NO_2^+ ions studied by threshold photoelectron-photoion coincidence techniques. *J. Phys. Chem. A* **1997**, *101*, 685−689.
(17) Tang, X. F.; Garcia, G. A.; Nahon, L. High resolution vibronic state-specific dissociation of NO_2^+ in the 10.0−15.5 eV energy range by synchrotron double imaging photoelectron photoion coincidence. *Phys. Chem. Chem. Phys.* **2020**, *22*, 1974−1982.
(18) Jarvis, G.; Song, Y.; Ng, C. Y.; Grant, E. A characterization of vibrationally and electronically excited NO_2^+ by high-resolution threshold photoionization spectroscopy. *J. Chem. Phys.* **1999**, *111*, 9568−9573.
(19) Chang, H. B.; Huang, M. B. A theoretical study on the electronic states and O-loss photodissociation of the NO_2^+ ion. *ChemPhysChem* **2009**, *10*, 582−589.
(20) Huang, X. C.; Valeev, E. F.; Lee, T. J. Comparison of one-particle basis set extrapolation to explicitly correlated methods for the calculation of accurate quartic force fields, vibrational frequencies, and spectroscopic constants: Application to H_2O, N_2H^+, NO_2^+, and C_2H_2. *J. Chem. Phys.* **2010**, *133*, 244108.
(21) Carlson, T. A. Angular dependence of vibrational structure in the photoelectron spectra of N_2 and O_2. *Chem. Phys. Lett.* **1971**, *9*, 23−26.
(22) Stephan, K.; Helm, H.; Kim, Y. B.; Seykora, G.; Ramler, J.; Grössl, M.; et al. Single and double ionization of nitrogen dioxide by electron impact from threshold up to 180 eV. *J. Chem. Phys.* **1980**, *73*, 303−308.
(23) Mueller, J. A.; Rogers, S. A.; Houston, P. L. Zero kinetic energy photofragment spectroscopy: The threshold dissociation of NO_2. *J. Phys. Chem. A* **1998**, *102*, 9666−9673.
(24) Monti, O. L. A.; Dickinson, H.; Mackenzie, S. R.; Softley, T. P. Rapidly fluctuating anisotropy parameter in the near-threshold photodissociation of NO_2. *J. Chem. Phys.* **2000**, *112*, 3699−3709.
(25) Dibeler, V. H.; Reese, R. M.; Krauss, M. Mass spectrometric study of the photoionization of small polyatomic molecules. *Adv. Mass Spectrom.* **1966**, *3*, 471.
(26) Dibeler, V. H.; Walker, J. A.; Liston, S. K. Mass spectrometric study of photoionization. VII. Nitrogen dioxide and nitrous oxide. *J. Res. Natl. Bur. Stand., Sect. A* **1967**, *71A*, 371−378.
(27) Clemmer, D. E.; Armentrout, P. B. Direct determination of the adiabatic ionization energy of NO_2 as measured by guided ion-beam mass spectrometry. *J. Chem. Phys.* **1992**, *97*, 2451−2458.
(28) Wilkinson, I.; Whitaker, B. J. Some remarks on the photodynamics of NO_2. *Annu. Rep. Prog. Chem., Sect. C: Phys. Chem.* **2010**, *106*, 274−304.
(29) Jost, R.; Nygard, J.; Pasinski, A.; et al. and Delon, A. The photodissociation threshold of NO_2: Precise determination of its energy and density of states. *J. Chem. Phys.* **1996**, *105*, 1287−1290.
(30) Jarvis, G. K.; Evans, M.; Ng, C. Y.; Mitsuke, K. Rotational resolved pulsed field ionization photoelectron study of $NO^+(X^1S^+, v^+ = 0−32)$ in the energy range of 9.24−16.80 eV. *J. Chem. Phys.* **1999**, *111*, 3058−3069.
(31) Chupka, W. A., Sandorfy, C., Ausloos, P. J., Robin, M. B., Eds. *Chemical Spectroscopy and Photochemistry in the VUV*. Reidel, Dordrecht, The Netherlands, 1974; Vol. 4.
(32) Toffoli, D.; Lucchese, R. R.; Lebech, M.; Houver, J. C.; Dowek, D. Molecular frame and recoil frame photoelectron angular distributions from dissociative photoionization of NO_2. *J. Chem. Phys.* **2007**, *126*, 054307.
(33) Tang, X. F.; Garcia, G. A.; Nahon, L. Dissociation of high-lying electronic states of NO_2^+ in the 15.5−20 eV region. *J. Phys. Chem. A* **2021**, *125*, 1517−1525.
(34) Tang, X. F.; Zhou, X. G.; Niu, M. L.; Liu, S. L.; Sun, J. D.; Shan, X. B.; Liu, F. Y.; Sheng, L. S. A threshold photoelectron-photoion coincidence spectrometer with double velocity imaging using synchrotron radiation. *Rev. Sci. Instrum.* **2009**, *80*, 113101.
(35) Wang, S. S.; Kong, R. H.; Shan, X. B.; Zhang, Y. W.; Sheng, L. S.; Wang, Z. Y.; Hao, L. Q.; Zhou, S. K. Performance of the atomic and molecular physics beamline at the National Synchrotron Radiation Laboratory. *J. Synchrotron Radiat.* **2006**, *13*, 415−420.
(36) Sztaray, B.; Baer, T. Suppression of hot electrons in threshold photoelectron photoion coincidence spectroscopy using velocity focusing optics. *Rev. Sci. Instrum.* **2003**, *74*, 3763−3768.
(37) Bodi, A.; Sztaray, B.; Baer, T.; Johnson, M.; Gerber, T. Data acquisition schemes for continuous two-particle time-of-flight coincidence experiments. *Rev. Sci. Instrum.* **2007**, *78*, 084102.
(38) Townsend, D.; Minitti, M. P.; Suits, A. G. Direct current slice imaging. *Rev. Sci. Instrum.* **2003**, *74*, 2530−2539.
(39) Frisch, M. J.; Trucks, G. W.; Schlegel, H. B.; Scuseria, G. E.; Robb, M. A.; Cheeseman, J. R.; Scalmani, G.; Barone, V.; Petersson, G. A.; Nakatsuji, H.; et al. *Gaussian 16*, Rev. A.03; Gaussian: Wallingford, CT, 2016.
(40) Mozhayskiy, V. A.; Krylov, A. I. *ezSpectrum*; http://iopenshell.usc.edu/downloads (accessed December 10, 2015).

https://doi.org/10.1021/acs.jpca.1c00701
J. Phys. Chem. A 2021, 125, 3316−3326

(41) Yu, T. P.; Wu, X. K.; Zhou, X. G.; Bodi, A.; Hemberger, P. Hydrogen migration as a potential driving force in the thermal decomposition of dimethoxymethane: New insights from pyrolysis imaging photoelectron photoion coincidence spectroscopy and computations. *Combust. Flame* **2020**, *222*, 123−132.
(42) Chen, Y.; Yu, T. P.; Wu, X. K.; Zhou, X. G.; Liu, S. L.; Liu, F. Y.; Dai, X. H. C-F and C-H bond cleavage mechanisms of trifluoromethane ion in low-lying electronic states: Threshold photoelectron-photoion coincidence imaging and theoretical investigations. *Phys. Chem. Chem. Phys.* **2020**, *22*, 13808−13817.
(43) Wu, X. K.; Zhou, X. G.; Hemberger, P.; Bodi, A. A guinea pig for conformer selectivity and mechanistic insights into dissociative ionization by photoelectron photoion coincidence: fluorocyclohexane. *Phys. Chem. Chem. Phys.* **2020**, *22*, 2351−2360.
(44) Wu, X. K.; Zhou, X. G.; Hemberger, P.; Bodi, A. Conformers, Electronic States and Diabolical Conical Intersections in the Valence Photoelectron Spectroscopy of Halocyclohexanes. *J. Chem. Phys.* **2020**, *153*, 054305.
(45) Nomoto, K.; Achiba, Y.; Kimura, K. HeI and HeII photoelectron study of N_2O_4. *Bull. Chem. Soc. Jpn.* **1979**, *52*, 1614−1618.
(46) Tang, X. F.; Garcia, G. A.; Nahon, L. High-resolution vacuum ultraviolet photodynamic of the nitrogen dioxide dimer $(NO_2)_2$ and the stability of its cation. *Phys. Chem. Chem. Phys.* **2020**, *22*, 21068−21073.
(47) Sztáray, B.; Bodi, A.; Baer, T. Modeling Unimolecular Reactions in Photoelectron Photoion Coincidence Experiments. *J. Mass Spectrom.* **2010**, *45*, 1233−1245.
(48) Shi, Y.; Li, Q. F.; Wang, H.; Dai, J. H.; Liu, S. L.; Ma, X. X. An approach to obtain the photofragment translational energy distribution from time-of-flight profile. *Acta Phys. Sin.* **2005**, *54*, 2418−2423.
(49) Seccombe, D. P.; Chim, R. Y. L.; Jarvis, G. K.; Tuckett, R. P. The use of threshold photoelectron-photoion coincidence spectroscopy to probe the spectroscopic and dynamic properties of the valence states of CCl_3F^+, CCl_3H^+. *Phys. Chem. Chem. Phys.* **2000**, *2*, 769−780.
(50) Weitzel, K. M.; Mahnert, J. The binding energies of small Ar, CO and N_2 cluster ions. *Int. J. Mass Spectrom.* **2002**, *214*, 175−212.
(51) Nenner, I.; Guyon, P. M.; Baer, T.; Govers, T. R. A threshold photoelectron-photoion coincidence study of the N_2O^+ dissociation between 15 and 20.5 eV. *J. Chem. Phys.* **1980**, *72*, 6587−6592.
(52) Chiang, Su-Yu.; Ma, C. Fragmentation of vibrationally velected N_2O^+ in state $\tilde{C}^2\Sigma^+$ from measurements of threshold photoelectron photoion coincidence. *J. Phys. Chem. A* **2000**, *104*, 1991−1996.
(53) Tang, X. F.; Niu, M. L.; Zhou, X. G.; Liu, S. L.; Liu, F. Y.; Shan, X. B.; Sheng, L. S. NO^+ formation pathways in dissociation of N_2O^+ ions at the $C^2\Sigma^+$ state revealed from threshold photoelectron-photoion coincidence velocity imaging. *J. Chem. Phys.* **2011**, *134*, 054312.
(54) Tang, X. F.; Zhou, X. G.; Wu, M. M.; Liu, S. L.; Liu, F. Y.; Shan, X. B.; Sheng, L. S. Dissociative photoionization of methyl chloride studied with threshold photoelectron-photoion coincidence velocity imaging. *J. Chem. Phys.* **2012**, *136*, 034304.
(55) Tang, X. F.; Zhou, X. G.; Wu, M. M.; Cai, Y.; Liu, S. L.; Sheng, L. S. Direct experimental evidences for dissociative photoionization of oxygen molecule via $^2\Sigma_u^{-2}$ ionic "Optical Dark" State. *J. Phys. Chem. A* **2012**, *116*, 9459−9465.
(56) Bartmess, J. E. *NIST Chemistry WebBook*; NIST: Gaithersburg, MD, 2005.
(57) Coxon, J. A.; Clyne, M. A. A.; Setser, D. W. Penning ionization optical spectroscopy: Metastable helium (He2^{3}S) with nitric oxide. *Chem. Phys.* **1975**, *7*, 255−266.
(58) Holdy, K. E.; Klotz, L. C.; Wilson, K. R. Molecular dynamics of photodissociation: quasidiatomic model for ICN. *J. Chem. Phys.* **1970**, *52*, 4588−4599.
(59) Tang, X. F.; Zhou, X. G.; Wu, M. M.; Gao, Z.; Liu, S. L.; Liu, F. Y.; Shan, X. B.; Sheng, L. S. Dissociation limit and dissociation dynamic of CF_4^+: Application of threshold photoelectron-photoion coincidence velocity imaging. *J. Chem. Phys.* **2013**, *138*, 094306.
(60) Wu, X. K.; Tang, G. Q.; Zhang, H. H.; Zhou, X. G.; Liu, S. L.; Liu, F. Y.; Sheng, L. S.; Yan, B. Cl-loss Dynamics in dissociative photoionization of CF_3Cl with threshold photoelectron-photoion coincidence imaging. *Phys. Chem. Chem. Phys.* **2018**, *20*, 4917−4925.

https://doi.org/10.1021/acs.jpca.1c00701
J. Phys. Chem. A 2021, 125, 3316−3326